Solar Energy Materials & Solar Cells 143 (2015) 354–359

Contents lists available at ScienceDirect

Solar Energy Materials & Solar Cells

journal homepage: www.elsevier.com/locate/solmat

Ambient stable large-area flexible organic solar cells using silver grid hybrid with vapor phase polymerized poly (3,4-Ethylenedioxythiophene) cathode

Yang Li [a,b], Lin Mao [a,b], Feng Tang [a], Qi Chen [a,g], Yixin Wang [a,b], Fengye Ye [a,c,g], Lei Chen [a,d], Yaowen Li [a,e], Dan Wu [a], Zheng Cui [f], Jinhua Cai [a,*], Liwei Chen [a,*]

[a] i-Lab, Suzhou Institute of Nano-Tech and Nano-Bionics (SINANO), Chinese Academy of Sciences, Suzhou 215123, China
[b] Nano Science and Technology Institute, University of Science and Technology of China (USTC), Suzhou 215123, China
[c] Department of Chemistry, University of Science and Technology of China, Hefei 230026, China
[d] Department of Chemistry, Shanghai University, Shanghai 200444, China
[e] College of Chemistry, Chemical Engineering and Materials Science, Soochow University, Suzhou 215123, China
[f] Division of Printed Electronics, Suzhou Institute of Nano-Tech and Nano-Bionics (SINANO), Chinese Academy of Sciences, Suzhou 215123, China
[g] Hefei National Laboratory for Physical Sciences at the Microscale, University of Science and Technology of China, Hefei 230026, China

ARTICLE INFO

Article history:
Received 16 March 2015
Received in revised form
9 July 2015
Accepted 14 July 2015
Available online 30 July 2015

Keywords:
Solar cell stability
Large-area solar cell
Organic solar cell
ITO-free
PSS-free

ABSTRACT

The presence of PSS in solution processed high conducting polymer PEDOT:PSS (PH1000) limits the reliability and lifetime of organic photovoltaic devices due to its acidic and hygroscopic nature. We have developed an alternative PSS-free transparent electrode, based on vapor-phase polymerized (VPP) PEDOT in combination with a current collecting silver grid. The hybrid electrode exhibits a low sheet resistance of 1.6 Ω/□ with an excellent bending proof performance. The power conversion efficiency (PCE) is 2.63% in a 1.21 cm^2 area device with a stacking structure of PET/Ag-grid/VPP-PEDOT/ZnO/poly[(9,9-bis(3-(N,N-dimethylamino)propyl)-2,7-fluorene)-alt-2,7-(9,9-dioctylfluorene)](PFN)/poly(3-hexylthiophene):[6,6]-phenyl-C61 butyric acid methyl ester (P3HT:PC_{61}BM)/MoO_3/Al. This efficiency is lower than, but comparable to the PCE (3.36%) of a control device with similar structure PET/Ag-grid/PH1000/ZnO/PFN/P3HT:PC_{61}BM/MoO_3/Al. A striking advantage using VPP-PEDOT to replace PH1000 is the high ambient stability of the device. The PCE of un-encapsulated devices after 120 h continuous exposure to ambient oxygen and moisture is retained at a 75% level of its initial value. These results suggest that the Ag grid/VPP-PEDOT is a promising alternative to ITO or high conducting PEDOT:PSS for realization of high efficiency, low cost and stable organic solar cells (OSCs).

© 2015 Elsevier B.V. All rights reserved.

1. Introduction

Effective utilization of solar power has become an intensively studied field due to the environmental effect and security concerns of fossil fuels [1–3]. Organic solar cells (OSCs) is a highly promising technology because of its light weight, easy process and low cost. The power conversion efficiency (PCE) of OSCs has lately exceeded 10% [4,5]. However, there are still two critical steps toward the commercialization of OSCs, one is to achieve large area OSCs on flexible substrate [6] and the other is to extend the working lifetime of OSCs to a rather acceptable time range [7].

Indium tin oxide (ITO), the most commonly used transparent electrode in OSCs, however, has several inherent drawbacks. The high cost of rare element indium [8], relatively high sheet resistance and poor mechanical property [9–11] hinder the effort of industrializing OSCs. The brittle ITO is apt to crack under tension, which makes it incompatible with low cost technologies like roll-to-roll printing and coating [12]. Various materials such as carbon nanotubes [13], graphene [14–16], metallic nanowires [17–20] and conductive polymer [21–23] thus have been proposed to replace ITO, but few of these alternatives alone can possess high conductivity and transmittance simultaneously, which are two essential factors for a material considered as electrode of OSCs.

Recently, we have presented a hybrid electrode consisted of high conducting poly (3,4-Ethylenedioxythiophene):poly(styrenesulfonate) (HC-PEDOT:PSS) and current collecting silver nanogrid [24,25]. The high transmittance and low sheet resistance of the hybrid electrode result in superior performance of OSC

* Corresponding authors.
E-mail addresses: jhcai2013@sinano.ac.cn (J. Cai), lwchen2008@sinano.ac.cn (L. Chen).

http://dx.doi.org/10.1016/j.solmat.2015.07.022
0927-0248/© 2015 Elsevier B.V. All rights reserved.

created with nitroPDF professional
download the free trial online at nitropdf.com/professional

devices as large as 1.21 cm^2. However, the hygroscopic nature of PSS in PEDOT:PSS film allows absorption of moisture from the atmosphere and results in an increased resistivity [26–28]. The PEDOT:PSS is also known to be easily photo-oxidized [29,30]. Moreover, the acidic PSS used in PEDOT:PSS may cause gradual erosion of the adjacent components such as the metal grid and the active material [31,32]. Therefore, the using of high conducting PEDOT:PSS as a component of the transparent electrode is detrimental to the stability of OSCs.

In comparison with solution processed PEDOT:PSS, the vapor-phase polymerization (VPP) PEDOT thin film usually shows enhanced conductivity and a smooth morphology [33,34]. Once incorporated with current collecting silver nanogrid, an electrode with low square resistance could be expected. The most appealing advantage of VPP-PEDOT is that it does not contain PSS, and thus shall be beneficial to stable OSCs with long lifetime.

Here we used VPP-PEDOT to replace HC-PEDOT:PSS in the hybrid cathode of large area, flexible OSCs with inverted structure of PET/Ag-grid/VPP-PEDOT/ZnO/poly [(9,9-bis(3-(N,N-dimethylamino)propyl)-2,7-fluorene)-alt-2,7-(9,9-dioctylfluorene)](PFN)/poly(3-hexylthiophene):[6,6]-phenyl-C61 butyric acid methyl ester (P3HT:$PC_{61}BM$)/MoO_3/Al. The resulting solar cells present a satisfactory power conversion efficiency (PCE) of 2.63%. Very importantly, the completely unencapsulated device retains 75% of its initial PCE after 120 h continuous exposure to ambient oxygen and moisture environment. We believe these results are highly intriguing for practical application of OSCs.

2. Experimental

The Ag-grid embedded PET (Suzhou NanoGrid Technology Co., Ltd.) was used as the substrate for VPP of the hybrid electrode. The structure of Ag-grid embedded in PET can be seen in our recent publication [24]. The hybrid electrodes were prepared by a VPP technique through procedures illustrated in Fig. 1(a). A 20 wt% solution of Fe(III) tosylate (technical grade, Aldrich) in n-butanol was used as the oxidizing agent. 0.5 mol of pyridine per mole of oxidant was used for base-inhibited VPP. To reduce the crystal formation of Fe(III) tosylate, the solution was spin-coated at 4500 rpm on Ag-grid embedded PET in a N_2 filled glovebox, and then baked at 55 °C overnight under vacuum. The monomer 3,4-ethylene dioxythiophene (EDOT) was obtained from Aldrich with a purity of 97%, and other chemicals were of analytical grade. The VPP process was conducted in the room humidity of ~40% with a N_2 flow at 150 mL/min. A jacketed reaction flask was used as the VPP chamber and its temperature was 55 °C, controlled by a super constant temperature bath (± 0.01 °C). The same VPP conditions were used to prepare a VPP-PEDOT on PET sample (PET/VPP-PEDOT) to evaluate the conductivity and optical transparency of VPP-PEDOT films.

Fig. 1(b) illustrates the structure of OSCs prepared in this study. ZnO nanoparticles and subsequent poly [(9,9-bis(3-(N,N-dimethylamino)propyl)-2,7-fluorene)-alt-2,7-(9,9-dioctylfluorene)] (PFN) layers were employed as the electron extraction layer. P3HT as donor material purchased from Luminescence Technology Corporation, $PC_{61}BM$ as acceptor material purchased from American Dye Source, Inc. were dissolved in 1,2-dichlorobenzene with a mixing ratio of 1:0.8 by weight and stirred for 12 h at 45 °C. Then, the active layers were obtained by spin coating of the blend solution at 600 rpm for 120 s followed by baking at 110 °C for 10 m. Then, MoO_3 and metal Al were thermally evaporated in a vacuum chamber through a shadow mask. The thickness of MoO_3, employed as the hole extraction, was about 10 nm; The thickness of Al, worked as top electrode, was about 100 nm. The effective cell area defined by the geometrical overlap between the bottom cathode electrode and top anode electrode was 1.21 cm^2.

Current density–voltage (J–V) characteristics of the solar cells under illumination of 100 mA/cm^2 white light from a Hg–Xe lamp filtered by a Newport 81094 Air Mass Filter were obtained using a Keithley 2635 A source meter. All the measurements were performed under ambient atmosphere at room temperature. Then without any encapsulation, these devices were stored in air and tested at intervals in 120 h to determine the device stability and the electrical performance, according to ISOS-L-1 conditions [35].

3. Results and discussion

The current-collecting silver nanogrid used in this study has been reported in our previous publication [24]. This investigation focuses on the application of VPP-PEDOT in the hybrid electrode. The VPP-PEDOT is used as an electrical connection between the cathode interlayer (ZnO/PFN) and Ag-grid, therefore we intend to make the VPP-PEDOT film as thin as possible for high optical transmittance and low electrical resistance. A 50 nm VPP-PEDOT film is the thinnest film we can obtain through VPP method. The transmittance spectra of Ag-grid, 50 nm VPP-PEDOT/Ag-grid and 150 nm PH1000/Ag-grid are presented in Fig. 2(a). A layer of 50 nm VPP-PEDOT blocks nearly 15% of the incident light, which is

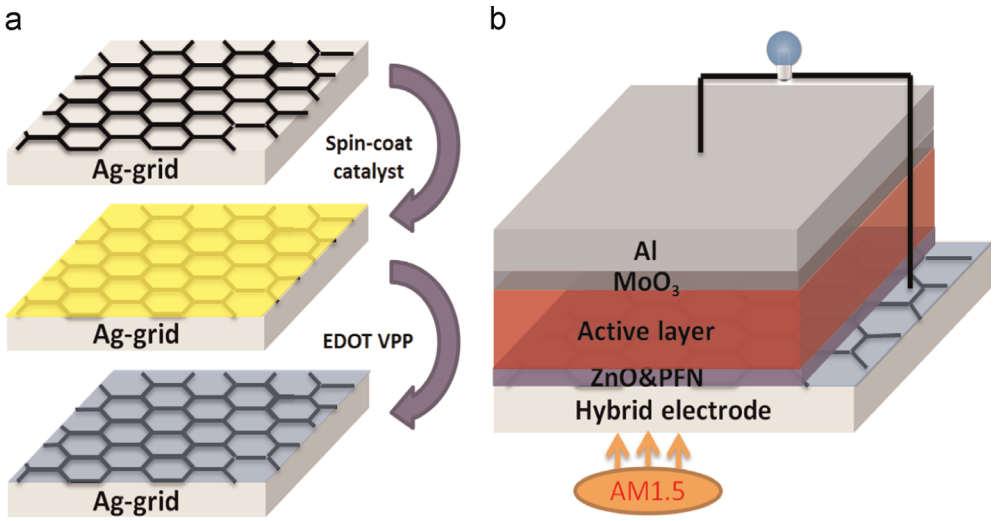

Fig.1. Schematic illustration of (a) procedures of preparing hybrid electrode; and (b) device configuration of hybri

created with nitroPDF professional
download the free trial online at nitropdf.com/professional

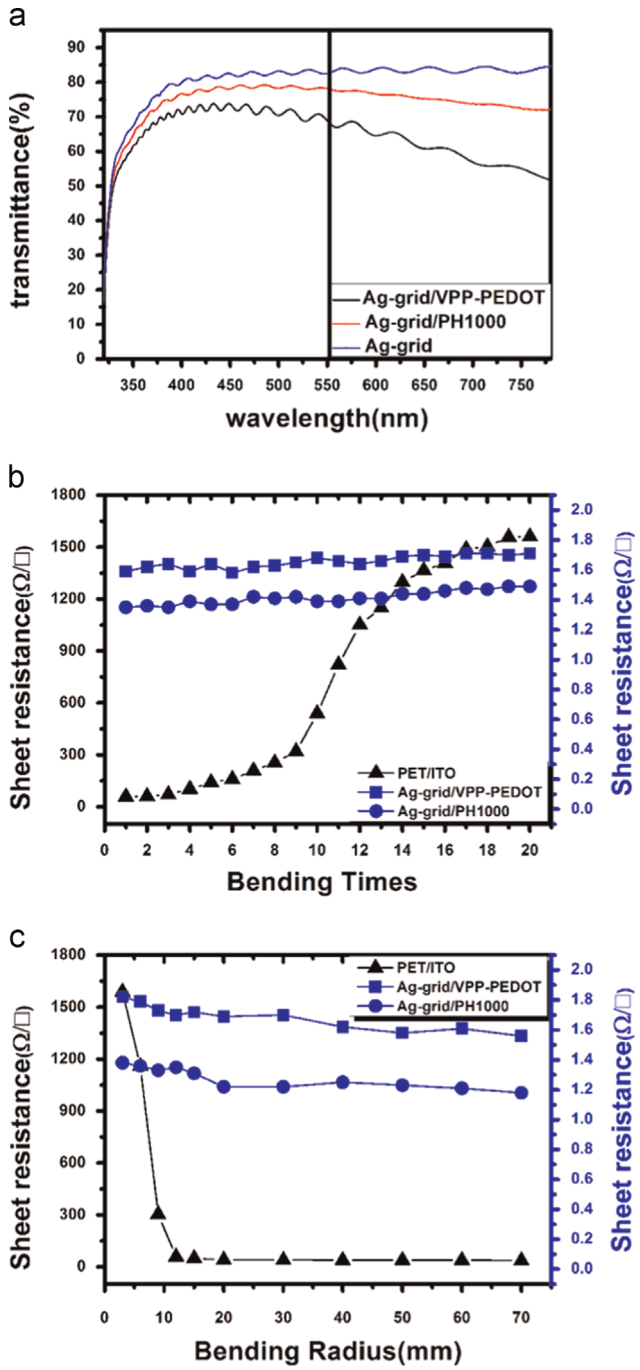

Fig.2. (a) Transmittance spectra of Ag-grid, Ag-grid/HC-PEDOT and Ag-grid/VPP-PEDOT; (b) dependence of sheet resistance on bending times at a radius of 12 mm of Ag-grid/ VPP-PEDOT and PET/ITO; (c) dependence of sheet resistance on bending radius (measured after fully relaxing) of Ag-grid/VPP-PEDOT and PET/ITO after the first bending.

higher than spin-casted films of PH1000; it also shows a relatively higher conductivity ($\sim$1000 S cm^{-1}) than PH1000 ($\sim$700 S cm^{-1}). The sheet resistance of the resulted VPP-PEDOT/Ag-grid hybrid electrode is 1.6 Ω/□, only a little higher than that of 150 nm PH1000/Ag-grid (1.2 Ω/□). Hereafter these two types of hybrid electrodes are tested in OSCs and compared for their performances.

A major advantage of polymers like PEDOT versus inorganic material is their superior flexibility. Fig. 2(b) shows the dependence of Ag-grid/VPP-PEDOT, Ag-grid/PH1000 and PET/ITO sheet resistances on bending times at a radius of 12 mm. After bending at a radius of 12 mm 20 times, the sheet resistances of Ag-grid/VPP-PEDOT and Ag-grid/PH1000 keep to be low and stable while that of PET/ITO becomes highly resistant in about 10 times bending. Fig. 2(c) shows the dependence of Ag-grid/VPP-PEDOT, Ag-grid/PH1000 and PET/ITO sheet resistances at various bending radii after the first bending. The sheet resistance of Ag-grid/VPP-PEDOT and Ag-grid/PH1000 is maintained at an excellent level of <2 Ω/□ even after bending at a radius of 3 mm. However, as comparison, the initial sheet resistance of PET/ITO is as high as 35 Ω/□ already and can further shoot up to over 1000 Ω/□ once bended at a radius less than 8 mm. This result highlights the feasibility of replacing ITO with Ag-grid/VPP-PEDOT in solar cells since lower sheet resistance means less electric energy wasted in electrodes and potentially better cell area scaling behavior without compromising the PCE [25].

OSCs devices with a stacking structure as illustrated in Fig. 1(c) were fabricated using the Ag-grid/VPP-PEDOT hybrid electrode. Similar devices using Ag-grid/PH1000 electrode were also prepared as controls. The *J–V* characteristics of the devices were measured under AM1.5 (100 mW/cm^2) white light illumination (Fig. 3(a)), and Fig. 3(b) shows the external quantum efficiency (EQE) curves of devices with Ag-grid/VPP-PEDOT and Ag-grid/PH1000 hybrid electrodes. The OSCs performance parameters are extracted and summarized in Table 1. The Ag-grid/VPP-PEDOT hybrid electrode based OSCs exhibit an open circuit voltage (V_{oc}) of 0.62 V, a short circuit current density (J_{sc}) of 8.15 mA/cm^2, a fill factor (FF) of 0.52 and a PCE of 2.63%, which is lower than the devices based on Ag-grid/PH1000 in J_{sc} and FF. The decrease in J_{sc} is mainly due to reduced optical transparency. To understand the reduction in FF, the *J–V* curves in Fig. 3(a) are fit using an one-diode equivalent circuit model [36]; and the extracted parameters: J_0 (reversed staturation current density of diode), n (ideality factor of diode), R_s (serial resistance), R_{sh} (shunt resistance) are listed also in Table 1. Although the square resistance of Ag-grid/VPP-PEDOT is larger than that of Ag-grid/PH1000, the serial resistance of Ag-gird/VPP-PEDOT device is smaller that of Ag-grid/PH1000 device. The reason is that the square resistance cannot completely characterize the current-collecting capability of film, especially in the cases where the current distribution in device is significantly different from that in the configuration for square resistance measurement. Since the serial resistance in Ag-grid/VPP-PEDOT device is lower than that in the control device, we can conclude that the decrease in FF is not due to changes in serial resistance. Similarly, we also exclude the shunt resistance as a factor for the drop of FF since the both shunt resistances are at same level. The large J_0 and n are responsible for the smaller FF in VPP-PEDOT devices. The large J_0 indicates the recombination is stronger in Ag-grid/VPP-PEDOT device than in Ag-grid/PH1000 device. The large n may indicate that more defects exist in Ag-grid/VPP-PEDOT device. The surface topography of VPP-PEDOT and PH1000 films are imaged with atomic force microscopy (AFM) (Fig. 4(a) and (b)). Both electrodes show uniform and smooth surfaces that are necessary to be used as the bottom cathode. The root mean square (RMS) roughness values measured by AFM are 4.5 nm and 2.2 nm for VPP-PEDOT and PH1000, respectively. The slightly higher roughness may result in non-ideal interfacial contact between adjacent layers, and could be the origin of large J_0 and n. Considering that the active area of these cells are as large as 1.21 cm^2, these OSCs have shown PCE better than many ITO electrode based devices with the same area, and thus can be deemed acceptable performances.

The major motivation of replacing PH1000 with VPP-PEDOT is to improve the stability of the resulting OSCs, which is a critical factor in evaluating the potential of a solar cell in practical applications. Here we monitor the ambient stability of the Ag-grid/PH1000 and Ag-grid/VPP-PEDOT

created with nitroPDF professional
download the free trial online at nitropdf.com/professional

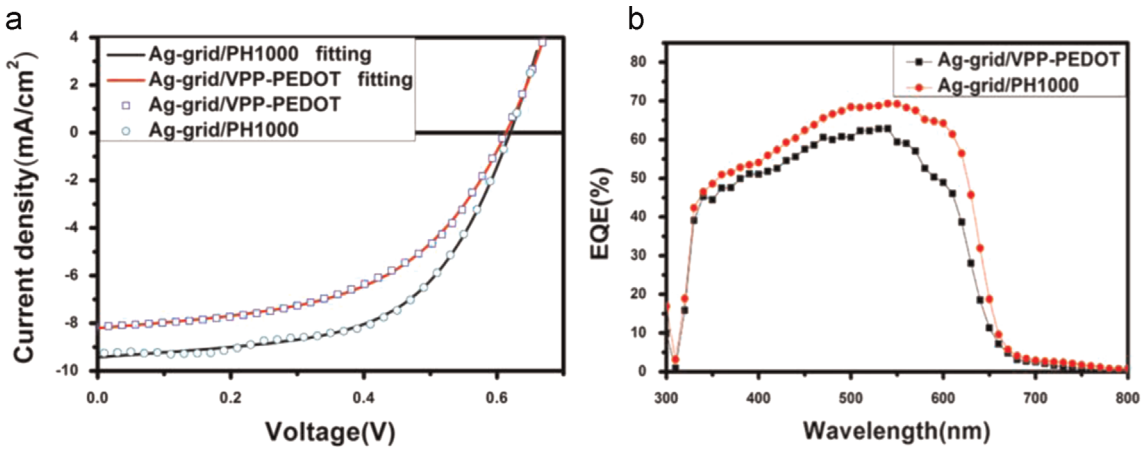

Fig.3. (a) *J–V* characteristics of P3HT:$PC_{61}BM$ OSCs based on Ag-grid/VPP-PEDOT and Ag-grid/PH1000 hybrid electrodes under AM 1.5, 100 mW/cm^2 white light illumination and their corresponding fits; (b) EQE spectra of the same devices.

Table 1
OSCs performances parameters of devices with different electrodes.

Bottom electrode	V_{oc} (V)	J_{sc} (mA/cm^2)	FF	PCE (%)	R_s (Ω cm^2)	R_{sh} (Ω cm^2)	J_0 (μA/cm^2)	n
Ag-grid/PH1000	0.62	9.50	0.57	3.36	4.86	504	1.25	2.68
Ag-grid/VPP-PEDOT	0.62	8.15	0.52	2.63	3.62	489	12.2	3.76

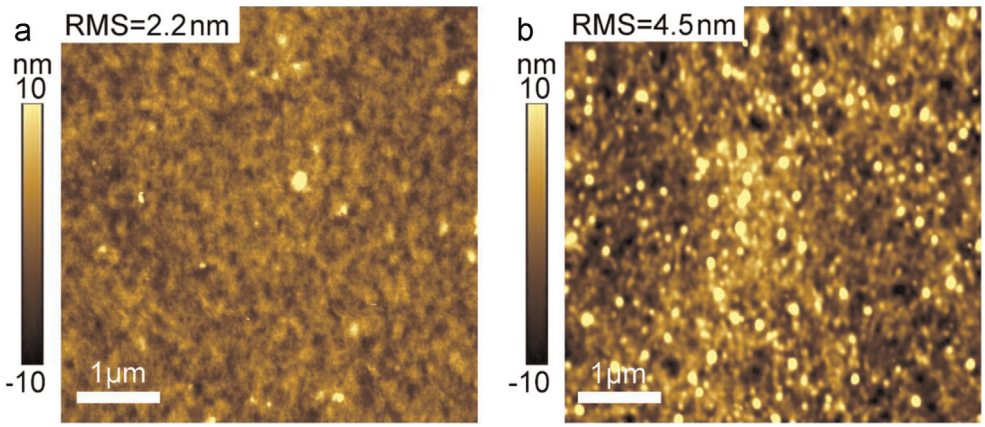

Fig.4. AFM images of (a) PH1000 film on Ag-grid substrate; (b) VPP-PEDOT film on Ag-grid substrate.

any encapsulation. The initial performance of the devices is acquired immediately after fabrication, and the devices are then tested once every two hours in the next six hours. As shown in Fig. 5, the V_{oc} of both types of devices are relatively constant, but the Ag-grid/PH1000 based device showed a drastic drop in J_{sc} from nearly 10 mA/cm^2 to 4 mA/cm^2, and a decreased FF from 55% to 40%. Meanwhile, J_{sc} and FF of Ag-grid/VPP-PEDOT based devices are still quite stable. During the next stage of observation, the devices are tested every 12 h for as long as 120 h. The Ag-grid/PH1000 based devices quickly degraded to reach a total failure in the first 12 h. On the contrary, Ag-grid/VPP-PEDOT based devices retain 75% of their initial PCE at the end of the 120 h.

The influence of interfacial layers on OPV stability has been an intensively investigated topic [37–45]. It has been reported that the absorption of water and oxygen due to the presence of PEDOT:PSS may accelerate the degradation of active layer and the oxidation of top electrode [26–32]. In conventional devices, the ITO electrode can be significantly eroded because of its direct contact with the PEDOT:PSS layer [38,39]. In most cases, PEDOT is applied in OPV devices along with PSS to form spin-cast thin-films; it is thus highly interesting to delineate the effect of the two components. The oxygen permeability of VPP PEDOT and its relationship with device stability have been studied by Andersen et al. [38,45] On the other hand, no PSS has been applied in OPV in its pure form, the effect of the acidic PSS in PEDOT:PSS on device stability has been controversial [40,41,44]. Although our results described above do not offer insights into the device degradation mechanism at a molecular level, these data offers important evidences that PSS in the PEDOT:PSS mixture is likely to be the major cause of device instability.

4. Conclusions

We have demonstrated that VPP-PEDOT coated silver grid can act as a hybrid transparent electrode for large area flexible OSCs with good stability. The Ag-grid/VPP-PEDOT hybrid electrode shows high optical transparency and good electrical conductivity. The PCE of Ag-grid/VPP-PEDOT hybrid electrode based device reaches 2.63% at a large device area (1.21 cm^2). Compared with the control electrode with HC-PEDOT (PH1000) on Ag-grid, Ag-grid/VPP-PEDOT based device exhib

created with nitroPDF professional
download the free trial online at nitropdf.com/professional

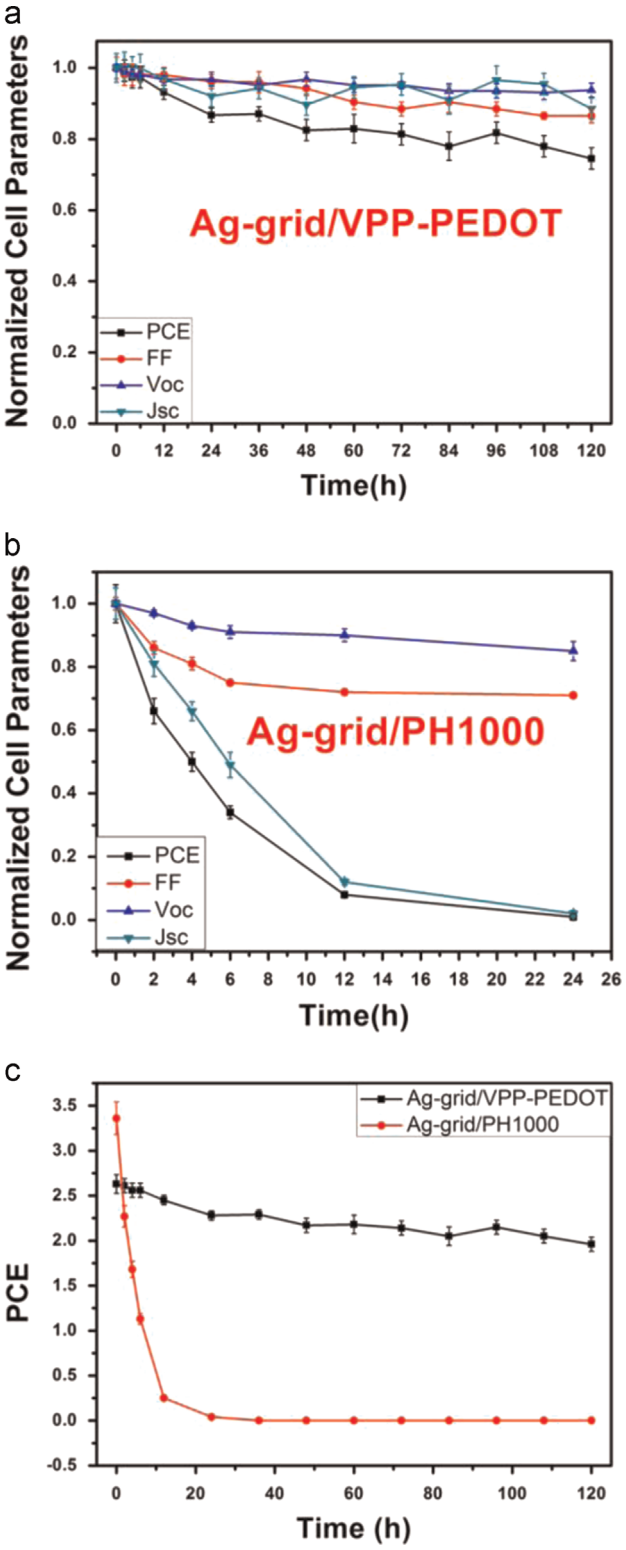

Fig.5. Aging characteristics of solar cells with Ag-grid/VPP-PEDOT hybrid electrodes or Ag-grid/HC-PEDOT hybrid electrodes. (a) Normalized cell parameters of devices with Ag-grid/VPP-PEDOT hybrid electrodes as functions of time; (b) normalized cell parameters of devices with Ag-grid/HC-PEDOT hybrid electrodes as functions of time; (c) PCE of the devices with two different kinds of hybrid electrodes as functions of time. All devices were tested under AM 1.5G simulated solar illumination without encapsulation. The error bars are sample standard deviations obtained from six independent measurements performed under the same conditions.

stability. After 120 h continuous exposure to the ambient environment, unencapsulated Ag-grid/VPP-PEDOT based devices still exhibit 75% of their initial efficiency. This study shows that the Ag-grid/VPP-PEDOT hybrid electrode combines multiple critical features including high electrical conductivity, optical transparency, mechanical flexibility, solution processability and most importantly, device stability, and therefore is highly promising in future high-throughput roll-to-roll manufacturing of large-area OSCs.

Acknowledgments

This work was supported by the National Natural Science Foundation of China (Nos: 91233104, 61376063, and 51473184). L. C. acknowledges the support from Jiangsu Provincial Natural Science Foundation (Grant no. BK20130006).

References

[1] B. Winther-Jensen, F.C. Krebs, High-conductivity large-area semi-transparent electrodes for polymer photovoltaics by silk screen printing and vapour-phase deposition, Sol. Energy Mater. Sol. Cells 90 (2006) 123–132.
[2] C. Lungenschmied, G. Dennler, H. Neugebauer, S.N. Sariciftci, M. Glatthaar, T. Meyer, A. Meyer, Flexible, long-lived, large-area, organic solar cells, Sol. Energy Mater. Sol. Cells 91 (2007) 379–384.
[3] G. Li, R. Zhu, Y. Yang, Polymer solar cells, Nat. Photon. 6 (2012) 153–161.
[4] Z. He, C. Zhong, S. Su, M. Xu, H. Wu, Y. Cao, Enhanced power-conversion efficiency in polymer solar cells using an inverted device structure, Nat. Photon. 6 (2012) 593–597.
[5] Z. He, C. Zhong, X. Huang, W.Y. Wong, H. Wu, L. Chen, S. Su, Y. Cao, Simultaneous enhancement of open-circuit voltage, short-circuit current density, and fill factor in polymer solar cells, Adv. Mater. 23 (2011) 4636–4643.
[6] F.C. Krebs, J. Fyenbo, M. Jørgensen, Product integration of compact roll-to-roll processed polymer solar cell modules: methods and manufacture using flexographic printing, slot-die coating and rotary screen printing, J. Mater. Chem. 20 (2010) 8994.
[7] J.A. Hauch, P. Schilinsky, S.A. Choulis, R. Childers, M. Biele, C.J. Brabec, Flexible organic P3HT:PCBM bulk-heterojunction modules with more than 1 year outdoor lifetime, Sol. Energy Mater. Sol. Cells 92 (2008) 727–731.
[8] Y. Leterrier, L. Médico, F. Demarco, J.A.E. Månson, U. Betz, M.F. Escolà, M. Kharrazi Olsson, F. Atamny, Mechanical integrity of transparent conductive oxide films for flexible polymer-based displays, Thin Solid Films 460 (2004) 156–166.
[9] T. Kamiya, H. Hosono, Material characteristics and applications of transparent amorphous oxide semiconductors, NPG Asia Mater. 2 (2010) 15–22.
[10] K.-H. Choi, J.-A. Jeong, J.-W. Kang, D.-G. Kim, J.K. Kim, S.-I. Na, D.-Y. Kim, S.-S. Kim, H.-K. Kim, Characteristics of flexible indium tin oxide electrode grown by continuous roll-to-roll sputtering process for flexible organic solar cells, Sol. Energy Mater. Sol. Cells 93 (2009) 1248–1255.
[11] M.G. Kim, M.G. Kanatzidis, A. Facchetti, T.J. Marks, Low-temperature fabrication of high-performance metal oxide thin-film electronics via combustion processing, Nat. Mater. 10 (2011) 382–388.
[12] D. Angmo, F.C. Krebs, Flexible ITO-free polymer solar cells, J. Appl. Polym. Sci. 129 (2012) 1–14.
[13] T.P. Tyler, R.E. Brock, H.J. Karmel, T.J. Marks, M.C. Hersam, Electronically monodisperse single-walled carbon nanotube thin films as transparent conducting anodes in organic photovoltaic devices, Adv. Energy Mater. 1 (2011) 785–791.
[14] Y. Zongyou, S. Shuangyong, S. Teddy, W. Shixin, H. Xiao, H. Qiyuan, L. YengMing, Z. Hua, Organic photovoltaic devices using highly flexible reduced graphene oxide films as transparent electrodes, ACS Nano 4 (2010) 5263–5268.
[15] L.G.D. Arco, Yi Zhang, C.W. Schlenker, K. Ryu, M.E. Thompson, C. Zhou, Continuous, highly flexible, and transparent graphene films by chemical vapor deposition for organic photovoltaics, ACS Nano 4 (2010) 2865–2873.
[16] Q. Zhang, X. Wan, F. Xing, L. Huang, G. Long, N. Yi, W. Ni, Z. Liu, J. Tian, Y. Chen, Solution-processable graphene mesh transparent electrodes for organic solar cells, Nano Res. 6 (2013) 478–484.
[17] L. Yang, T. Zhang, H. Zhou, S.C. Price, B.J. Wiley, W. You, Solution-processed flexible polymer solar cells with silver nanowire electrodes, ACS Appl. Mater. Interfaces 3 (2011) 4075–4084.
[18] D.S. Leem, A. Edwards, M. Faist, J. Nelson, D.D. Bradley, J.C. de Mello, Efficient organic solar cells with solution-processed silver nanowire electrodes, Adv. Mater. 23 (2011) 4371–4375.
[19] Z. Yu, L. Li, Q. Zhang, W. Hu, Q. Pei, Silver nanowire-polymer composite electrodes for efficient polymer sola

created with nitroPDF professional
download the free trial online at nitropdf.com/professional

[20] C. Mayousse, C. Celle, A. Carella, J.-P. Simonato, Synthesis and purification of long copper nanowires. Application to high performance flexible transparent electrodes with and without PEDOT:PSS, Nano Res. 7 (2014) 315–324.
[21] T. Aernouts, P. Vanlaeke, W. Geens, J. Poortmans, P. Heremans, S. Borghs, R. Mertens, R. Andriessen, L. Leenders, Printable anodes for flexible organic solar cell modules, Thin Solid Films 451–452 (2004) 22–25.
[22] C.-K. Cho, W.-J. Hwang, K. Eun, S.-H. Choa, S.-I. Na, H.-K. Kim, Mechanical flexibility of transparent PEDOT:PSS electrodes prepared by gravure printing for flexible organic solar cells, Sol. Energy Mater. Sol. Cells 95 (2011) 3269–3275.
[23] Y.H. Kim, C. Sachse, M.L. Machala, C. May, L. Müller-Meskamp, K. Leo, Highly conductive PEDOT:PSS electrode with optimized solvent and thermal post-treatment for ITO-free organic solar cells, Adv. Funct. Mater. 21 (2011) 1076–1081.
[24] Y. Li, L. Mao, Y. Gao, P. Zhang, C. Li, C. Ma, Y. Tu, Z. Cui, L. Chen, ITO-free photovoltaic cell utilizing a high-resolution silver grid current collecting layer, Sol. Energy Mater. Sol. Cells 113 (2013) 85–89.
[25] L. Mao, Q. Chen, Y. Li, Y. Li, J. Cai, W. Su, S. Bai, Y. Jin, C.-Q. Ma, Z. Cui, L. Chen, Flexible silver grid/PEDOT:PSS hybrid electrodes for large area inverted polymer solar cells, Nano Energy 10 (2014) 259–267.
[26] H.S. Kang, H.S. Kang, J.K. Lee, J.W. Lee, J. Joo, J.M. Ko, M.S. Kim, J.Y. Lee, Humidity-dependent characteristics of thin film poly(3,4-ethylenedioxythiophene) field-effect transistor, Synth. Met. 155 (2005) 176–179.
[27] J. Huang, P.F. Miller, J.S. Wilson, A.Jd Mello, J.Cd Mello, D.D.C. Bradley, Investigation of the effects of doping and post-deposition treatments on the conductivity, morphology, and work function of Poly(3,4-ethylenedioxythiophene)/Poly(styrene sulfonate) films, Adv. Funct. Mater. 15 (2005) 290–296.
[28] K. Kawano, R. Pacios, D. Poplavskyy, J. Nelson, D.D.C. Bradley, J.R. Durrant, Degradation of organic solar cells due to air exposure, Sol. Energy Mater. Sol. Cells 90 (2006) 3520–3530.
[29] K. Jeuris, L. Groenendaal, H. Verheyen, F. Louwet, F.C.D. Schryver, Light stability of 3,4-ethylenedioxythiophene-based derivatives, Synth. Met. 132 (2003) 289–295.
[30] M. Vázquez, J. Bobacka, A. Ivaska, A. Lewenstam, Influence of oxygen and carbon dioxide on the electrochemical stability of poly(3,4-ethylenedioxythiophene) used as ion-to-electron transducer in all-solid-state ion-selective electrodes, Sens. Actuators B: Chem. 82 (2003) 7–13.
[31] J.K.J.v. Duren, J. Loos, F. Morrissey, C.M. Leewis, K.P.H. Kivits, L.J.v. IJzendoorn, M.T. Rispens, J.C. Hummelen, R.A.J. Janssen, In-situ compositional and structural analysis of plastic solar cells, Adv. Funct. Mater. 12 (2002) 665–669.
[32] K. Norrman, M.V. Madsen, S.A. Gevorgyan, F.C. Krebs, Degradation patterns in water and oxygen of an inverted polymer solar cell, J. Am. Chem. Soc. 132 (2010) 16883–16892.
[33] P.A. Levermore, L. Chen, X. Wang, R. Das, D.D.C. Bradley, Fabrication of highly conductive Poly(3,4-ethylenedioxythiophene) films by vapor phase polymerization and their application in efficient organic light-emitting diodes, Adv. Mater. 19 (2007) 2379–2385.
[34] D. Wu, J. Zhang, W. Dong, H. Chen, X. Huang, B. Sun, L. Chen, Temperature dependent conductivity of vapor-phase polymerized PEDOT films, Synth. Met. 176 (2013) 86–91.
[35] M.O. Reese, S.A. Gevorgyan, M. Jørgensen, E. Bundgaard, S.R. Kurtz, D.S. Ginley, D.C. Olson, M.T. Lloyd, P. Morvillo, E.A. Katz, A. Elschner, O. Haillant, T.R. Currier, V. Shrotriya, M. Hermenau, M. Riede, K.R. Kirov, G. Trimmel, T. Rath, O. Inganäs, F. Zhang, M. Andersson, K. Tvingstedt, M. Lira-Cantu, D. Laird, C. McGuiness, S. Gowrisanker, M. Pannone, M. Xiao, J. Hauch, R. Steim, D.M. DeLongchamp, R. Rösch, H. Hoppe, N. Espinosa, A. Urbina, G. Yaman-Uzunoglu, J.-B. Bonekamp, A.J.J.M. van Breemen, C. Girotto, E. Voroshazi, F.C. Krebs, Consensus stability testing protocols for organic photovoltaic materials and devices, Sol. Energy Mater. Solar Cells 95 (2011) 1253–1267.
[36] J. Cai, N. Satoh, M. Yanagida, L. Han, Successive large perturbation method for the elimination of initial value dependence in I-V curve fitting, Rev. Sci. Instrum. 80 (2009) 115111.
[37] A. Seemann, H.J. Egelhaaf, C.J. Brabec, J.A. Hauch, Influence of oxygen on semi-transparent organic solar cells with gas permeable electrodes, Org. Electron. 10 (2009) 1424–1428.
[38] V.M. Drakonakis, A. Savva, M. Kokonou, S.A. Choulis, Investigating electrodes degradation in organic photovoltaics through reverse engineering under accelerated humidity lifetime conditions, Sol. Energy Mater. Sol. Cells 130 (2014) 544–550.
[39] M.P. de Jong, L.J. van IJzendoorn, M.J.A. deVoigt, Stability of the interface between indium-tin-oxideand poly(3,4-ethylenedioxythiophene)/poly(styrenesulfonate) in polymer light-emitting diodes, Appl. Phys. Lett. 77 (2000) 2255–2257.
[40] E. Voroshazi, B. Verreet, A. Buri, R. Muller, D. Nuzzo, P. Heremans, Influence of cathode oxidation via the hole extraction layer in polymer:fullene solar cells, Org. Electron. 12 (2011) 736–744.
[41] Y. Meng, Z. Hu, N. Ai, Z. Jiang, J. Wang, J. Peng, Y. Cao, Improving the stability of bulk heterojunction solar cells by inicorporating pH-Neutral PEDOT:PSS as the hole transport layer, ACS Appl. Mater. Interfaces 6 (2014) 5122–5129.
[42] T. Yamanari, T. Taima, J. Sakai, J. Tsukamoto, Y. Yoshida, Effect of buffer layers on stability of polymer-based organic solar cells, Jpn. J. Appl. Phys. 49 (2010) 01AC02.
[43] M. Jørgensen, K. Norrman, F.C. Krebs, Stability/Degradation of polymer solar cells, Sol. Energy Mater. Sol. Cells 92 (2008) 686–714.
[44] E. Andreoli, K. Liao, A. Haldar, N.J. Alley, S.A. Curran, PPy:PSS as alternative to PEDOT:PSS in organic photovoltaics, Synth. Met. 185–186 (2013) 71–78.
[45] M. Andersen, J.E. Carle´, N. Cruys-Bagger, M.R. Lilliedal, Mark A. Hammond, B. Winther-Jensen, F.C. Krebs, Transparent anodes for polymer photovoltaics: oxygen permeability of PEDOT, Sol. Energy Mater. Sol. Cells 91 (2007) 539–543.

created with nitroPDF professional
download the free trial online at nitropdf.com/professional